JOURNAL OF SOLID STATE CHEMISTRY 98, 323–329 (1992)

Zirconolite $CaZr_{0.92}Ti_{2.08}O_7$ from 294 to 1173 K

ROBERT W. CHEARY

School of Physical Sciences, University of Technology, Sydney, P.O. Box 123, Broadway, New South Wales, Australia 2007

Received October 28, 1991

High-resolution neutron powder diffraction data were collected from the monoclinic zirconolite $CaZr_{0.92}Ti_{2.08}O_7$ at temperatures from 294 to 1173 K. The structural parameters of this compound, which were derived by Rietveld refinement, are not substantially affected by temperature. The lattice parameters increase with temperature and the expansion is essentially isotropic. With the possible exception of the $Ti(1)O_6$ octahedron, which has more or less the same size over the complete temperature range, all the oxygen polyhedra expand more or less uniformly with temperature. The weighted mean thermal parameter fits a Debye function with $\theta_m = 535 \pm 20$ K superimposed onto a temperature independent term with an RMS displacement of 0.27 Å^2 arising from static disorder.

1. Introduction

Zirconolite is one of the major phases in the polytitanate ceramic known as SYNROC which is being developed as a host for nuclear waste. This ceramic incorporates the waste atoms in solid solution and each of the component phases accommodates a particular range of elements. Zirconolites accommodate the lanthanide and actinide group of elements (*1*). In nature, zirconolites can exist with a significant proportion of dissolved uranium and thorium (*2*) and the structure has withstood the effects of high level doses of alpha radiation without significant degradation (*3*).

The nominal composition of zirconolite is $CaZrTi_2O_7$, but it is stable over a range of Ti/Zr concentrations as $CaZr_xTi_{3-x}O_7$, with x from 0.85 to 1.30 (*4*). Pyatenko and Pudovkina (*5*) first identified zirconolite as an anion deficient superstructure derived from eight fluorite subcells, $Ca_8Zr_8Ti_{16}O_{56}\otimes_8$, where $\otimes$ is a vacancy. Over its solid solution range the structure adopts the monoclinic space group $C2/c$ (*6*) with the cell parameters $a \approx 12.44$ Å, $b \approx 7.28$ Å and $\beta \approx 100.5°$ remaining substantially unchanged by the Ti/Zr ratio. Only c changes significantly (>0.02 Å) going from 11.34 Å at $x = 0.85$ to 11.49 Å at $x = 1.30$.

Zirconolite is a layer structure with TiO_6 octahedra forming an hexagonal tungsten bronze motif as (001) planes (*7*). Ca and Zr form in sheets between layers of TiO_6 octahedra, and are ordered in rows along $[1\bar{1}0]$ at $z = 0$ and along [110] at $z = 0.5$ (see Fig. 1a).The large Ca ions sit in distorted CaO_8 cubes with an average Ca–O bond length ~2.46 Å, whilst Zr occupy smaller sites in ZrO_7 polyhedra in which the mean Zr–O bond length ~2.17 Å (see Fig. 1b). Together the Ca and Zr sites are capable of accommodating all the trivalent rare earth lanthanides. Large ions, such as Nd^{3+} with $R = 1.26$ Å (*8*), preferentially occupy the

0022-4596/92 $5.00

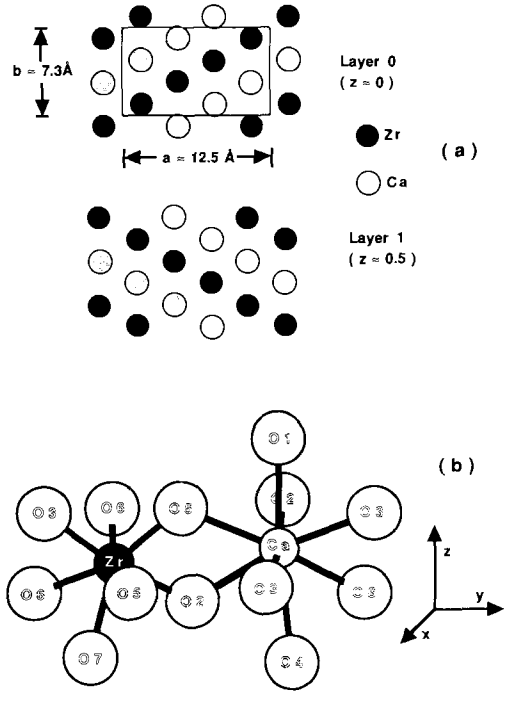

FIG. 1. (a) (001) layers at $z \approx 0$ and $z \approx 0.5$ in zirconolite showing the arrangement of Ca and Zr sites, and (b) adjacent CaO_8 and ZrO_7 polyhedra in zirconolite.

Ca sites, whereas smaller ions, such as Yb^{3+} with $R = 1.11$ Å, tend to occupy both sites equally (*1*). Intermediate sized ions, including Gd^{3+} and Dy^{3+}, tend to be partitioned unequally but weighted toward the Ca sites.

Selected area electron diffraction (*7*) reveals that rare earth substitution in zirconolites generates twinning faults particularly with large substituted ions. Fielding and White (*1*) have suggested that these faults are associated with clustering of the substituted ions. At substitution levels of up to 0.25 ions/cell, the substituted ions are randomly distributed and very few twinning faults form. Between 0.25 and 0.35 substituted ions/cell, the monoclinic zirconolite-2M structure forms intergrowths with the polytype trigonal zirconolite-3T structure (for nomenclature definitions see (*9*)). The essential difference between monoclinic and trigonal is that the repeat distance in the monoclinic c direction increases from 2 to 3 Ca/Zr sheets. When more than 0.75 rare earth ions/cell are substituted, cubic pyrochlore becomes the dominant phase.

As yet no systematic quantitative studies have been carried out to determine the crystal chemical characteristics of substituted zirconolite and in particular:

(i) the manner in which rare earth ions partition amongst the Ca and Zr sites,

(ii) the associated changes in both the lattice and structural parameters, and

(iii) the effect of high temperatures on the structure.

The present investigation is the first step of such an investigation and addresses the effects of temperature on the structural characteristics of unsubstituted zirconolite. This is of importance to the development of SYNROC to demonstrate that the zirconolite structure retains its structural integrity well above the temperatures it would have to endure when laden with nuclear waste. High-resolution neutron powder diffraction data have been collected from monoclinic $CaZr_{0.92}Ti_{2.08}O_7$ at temperatures from 294 to 1173 K. This technique was adopted because neutrons, unlike X rays, are sensitive to the oxygen and give reasonably accurate cation and oxygen structural parameters on refinement. Rietveld analysis was used to derive the structural parameters at each temperature. This paper discusses the changes in lattice parameters, bond lengths, and thermal vibrations with temperature.

2. Experimental Procedures and Rietveld Refinement

A 15-g polycrystalline sample of zirconolite was prepared for neutron diffraction by mixing the starting materials $CaCO_3$, ZrO_2, and TiO_2 in the ratio 1 : 1 : 2. This was done

by forming a slurry of these compounds with ethanol and then ball-milling for 20 min. After evaporating off the ethanol, the mixture was pressed into a large pellet and calcined at 1400 K for 4 hr. The pellet was then ground, converted to an ethanol slurry, and once again placed in a ball mill. After drying and being formed into a pellet, the sample was fired in air at 1650 K for 12 hr and allowed to cool slowly over a 24-hr period.

Fragments of the specimen were analysed on a JEOL 35C scanning electron microscope and on an Apex X-ray powder diffractometer. The SEM revealed a well crystallized material with a particle size range from 0.5 to 2 μm. X-ray powder diffraction confirmed that the specimen was at least 95% zirconolite. Weak traces of $CaTiO_3$ and ZrO_2 were observed, but only to the extent that the strongest diffraction lines of these impurities could be clearly identified. This is consistent with fact that the c lattice parameter obtained from the X-ray pattern, $c \approx 11.375$ Å, is slightly different from that expected for $CaZrTi_2O_7$ on the assumption that c is linear across the solid solution range. Using the c parameters given in (*4*) for $CaZr_xTi_{3-x}O_7$ at $x = 0.85$ and $x = 1.30$, the actual zirconolite prepared corresponds to $x \approx 0.95$. This composition is very close to the composition adopted which was given by Rietveld refinement of the neutron powder data, namely $CaZr_{0.92}Ti_{2.08}O_7$. X-ray microanalysis on the SEM at 15 kV was also used to estimate the composition of the zirconolite, but the results were judged to be inaccurate because of the poor reproducibility from crystallite to crystallite and the relatively small crystallite size ($\sim$1 μm).

Neutron diffraction data were collected using the eight detector high-resolution powder diffractometer on the HIFAR reactor at the Australian Nuclear Science and Technology Organisation (*10*). The wavelength used for the measurements was 1.891654 Å. This value was obtained by calibrating the diffractometer using a standard Si powder. Before measurement the zirconolite specimen was finely ground in a tungsten carbide ball mill, sieved through a 38-μm mesh and annealed at 1200 K for 4 hr to remove any strains set up by ball milling. Diffraction patterns were collected at temperatures of 294, 429, 573, 723, 873, 1023, and 1173 K. At room temperature (294 K), the 15-g specimen was packed into a 20-mm diameter V can mounted onto the rotating stage of the diffractometer. Count data were collected from $2\theta = 0°$ to 150° at intervals of 0.05° 2θ for fixed monitor counts. For all measurements above room temperature the specimen was packed into a thin-walled stainless steel canister. The high-temperature attachment on the diffractometer consisted of an evacuated alumina tube wound with Kanthal wire and insulated with ceramic wool. A chromel/alumel thermocouple was inserted into the specimen through the lid of the stainless steel canister. The temperature stability of the controller was typically $\pm$ 2°C. Count data from the high temperature specimens were recorded over the angular range $2\theta = 0$ to 150° at 0.1° 2θ intervals.

Rietveld refinement of the data was carried out using the program developed by Wiles and Young (*11*) and extensively modified by Howard and Hill (*12*). In the refinement the profiles were fitted by a pseudo-Voigt function with an angular dependent pseudo-Voigt parameter $\gamma = \gamma_0 + \gamma_1\ 2\theta + \gamma_2\ 2\theta^2$. An asymmetry term is also included in the refinement to represent the effects of vertical beam divergence (*13*). The data were corrected for zero 2θ error in the refinement and the background was fitted to a function of the form $b_0 + b_1\ 2\theta + b_2\ 2\theta^2 + b_3/2\theta$. Close inspection of the diffraction data revealed three very weak peaks from ZrO_2 and $CaTiO_3$, as well as prominent peaks from

TABLE I

STRUCTURAL PARAMETERS AND LATTICE PARAMETERS (in Å) FOR $CaZr_{0.92}Ti_{2.08}O_7$ OBTAINED FROM RIETVELD REFINEMENT TOGETHER WITH THE PATTERN GOODNESS OF FIT R_{wp}

Site		Temp (K)						
		294	429	573	723	873	1023	1173
Ca	x	0.3733(8)	0.3731(7)	0.3730(7)	0.3726(10)	0.3729(10)	0.3733(9)	0.3721(9)
	y	0.1257(22)	0.1267(22)	0.1293(22)	0.1228(29)	0.1192(25)	0.1192(24)	0.1187(23)
	z	0.4979(8)	0.4971(8)	0.4977(8)	0.4963(10)	0.4984(10)	0.4973(9)	0.4980(10)
	B	0.94(17)	0.93(16)	0.99(16)	1.08(24)	1.27(25)	1.80(22)	1.56(25)
Zr	x	0.1237(6)	0.1229(6)	0.1230(6)	0.1231(8)	0.1228(8)	0.1219(7)	0.1230(9)
	y	0.1219(15)	0.1229(15)	0.1244(15)	0.1244(22)	0.1242(20)	0.1218(17)	0.1232(19)
	z	−0.0247(5)	−0.0250(5)	−0.0243(6)	−0.0232(7)	−0.0233(7)	−0.0246(6)	−0.0229(7)
	B	0.12(14)	0.34(14)	0.47(15)	0.63(21)	1.07(21)	0.66(17)	1.68(21)
Ti1	x	0.2515(15)	0.2487(15)	0.2494(16)	0.2492(19)	0.2488(17)	0.2454(15)	0.2454(17)
	y	0.1202(48)	0.1246(48)	0.1131(38)	0.1161(72)	0.1331(53)	0.1265(54)	0.1216(53)
	z	0.7495(13)	0.7486(13)	0.7506(14)	0.7514(17)	0.7505(16)	0.7506(14)	0.7496(16)
	B	0.16(20)	0.61(20)	0.68(27)	0.85(40)	0.54(35)	0.39(28)	0.81(34)
Ti2	x	0.4663(27)	0.4663(29)	0.4665(30)	0.4619(34)	0.4615(34)	0.4672(35)	0.4634(39)
	y	0.0375(35)	0.0422(38)	0.0415(40)	0.0433(43)	0.0399(44)	0.0325(46)	0.0473(51)
	z	0.2550(38)	0.2528(38)	0.2553(40)	0.2532(47)	0.2461(49)	0.2517(51)	0.2489(59)
	B	1.80(90)	3.00(95)	2.78(90)	2.4(1.3)	2.5(1.2)	3.8(1.2)	4.6(1.5)
Ti3	y	0.1441(32)	0.1408(34)	0.1432(33)	0.1470(43)	0.1436(46)	0.1477(46)	0.1495(40)
	B	−0.12(35)	0.48(37)	0.37(36)	0.32(54)	1.39(60)	1.07(48)	0.76(50)
O1	x	0.3034(6)	0.3038(6)	0.3036(7)	0.3037(8)	0.3041(8)	0.3023(8)	0.3028(8)
	y	0.1245(17)	0.1239(17)	0.1253(18)	0.1247(22)	0.1240(20)	0.1220(20)	0.1245(21)
	z	0.2796(7)	0.2794(7)	0.2800(7)	0.2788(8)	0.2788(8)	0.2774(9)	0.2783(9)
	B	1.34(18)	1.53(18)	1.82(18)	1.58(26)	1.86(26)	2.46(23)	2.59(25)
O2	x	0.4717(7)	0.4703(7)	0.4708(8)	0.4708(10)	0.4693(10)	0.4699(9)	0.4712(10)
	y	0.1398(18)	0.1385(18)	0.1354(19)	0.1354(26)	0.1431(22)	0.1388(22)	0.1455(24)
	z	0.1041(6)	0.1022(6)	0.1032(6)	0.1037(8)	0.1038(8)	0.1034(8)	0.1040(9)
	B	1.82(21)	1.87(19)	2.17(21)	2.63(33)	3.01(33)	2.95(26)	3.74(32)
O3	x	0.2083(8)	0.2081(8)	0.2071(8)	0.2077(10)	0.2089(10)	0.2067(10)	0.2074(11)
	y	0.0902(13)	0.0904(13)	0.0920(14)	0.0937(17)	0.0952(17)	0.0921(17)	0.0948(18)
	z	0.5746(8)	0.5742(8)	0.5740(8)	0.5726(10)	0.5711(9)	0.5740(9)	0.5720(11)
	B	0.97(21)	1.11(19)	1.61(21)	1.35(31)	1.34(29)	2.30(27)	2.79(32)
O4	x	0.3979(8)	0.3941(7)	0.3972(8)	0.3982(9)	0.3967(9)	0.3971(9)	0.3968(10)
	y	0.1660(11)	0.1647(11)	0.1656(11)	0.1637(14)	0.1646(14)	0.1633(13)	0.1648(15)
	z	0.7188(8)	0.7198(8)	0.7208(8)	0.7192(9)	0.7202(9)	0.7192(9)	0.7193(10)
	B	0.77(21)	0.79(21)	0.84(19)	0.66(19)	0.79(26)	1.33(23)	1.78(28)
O5	x	0.7075(7)	0.7087(7)	0.7082(7)	0.7090(9)	0.7081(9)	0.7100(8)	0.7086(9)
	y	0.1728(11)	0.1746(11)	0.1737(11)	0.1756(15)	0.1778(15)	0.1764(14)	0.1762(15)
	z	0.5838(7)	0.5836(8)	0.5836(8)	0.5844(9)	0.5837(10)	0.5855(9)	0.5861(10)
	B	0.89(24)	1.09(22)	1.00(22)	1.09(33)	1.64(33)	1.62(28)	2.02(32)
O6	x	−0.0019(6)	−0.0020(6)	−0.0031(6)	−0.0032(8)	−0.0029(8)	−0.0032(7)	−0.0028(8)
	y	0.1252(17)	0.1238(17)	0.1220(17)	0.1235(21)	0.1259(20)	0.1229(19)	0.1275(20)
	z	0.4209(7)	0.4198(7)	0.4198(7)	0.4198(8)	0.4197(9)	0.4200(8)	0.4205(9)
	B	1.04(18)	1.01(16)	1.05(17)	0.84(24)	1.57(26)	1.31(20)	1.80(24)
O7	x	0.1135(9)	0.1132(9)	0.1126(9)	0.1124(12)	0.1108(12)	0.1114(11)	0.1110(12)
	y	0.0559(10)	0.0540(11)	0.0542(11)	0.0518(14)	0.0518(14)	0.0512(14)	0.0521(15)
	z	0.7901(9)	0.7914(9)	0.7911(9)	0.7935(12)	0.7930(12)	0.7920(11)	0.7918(12)
	B	1.33(22)	1.20(21)	1.42(20)	2.27(32)	2.38(32)	2.50(28)	2.68(31)
	a	12.4425(6)	12.4572(5)	12.4768(5)	12.4970(8)	12.5204(8)	12.5401(7)	12.5614(8)
	b	7.2722(3)	7.2801(3)	7.2895(3)	7.2986(5)	7.3093(5)	7.3187(4)	7.3288(4)
	c	11.3783(5)	11.3909(5)	11.4069(5)	11.4238(7)	11.4423(7)	11.4556(6)	11.4721(7)
	β	100.564(2)	100.563(2)	100.569(2)	100.580(3)	100.587(3)	100.600(2)	100.617(3)
	% R_{wp}	6.8	5.1	5.0	4.8	4.7	4.7	4.6
	% R_{wp}^{exp}	5.4	3.1	3.1	3.2	3.2	3.1	3.1
	% R_B	1.8	2.0	1.7	1.6	1.7	1.6	1.4

Note. The standard errors quoted in parenthesis are given by refinement and are based on the counting statistics. The isotropic temperature factors B are in Å^2.

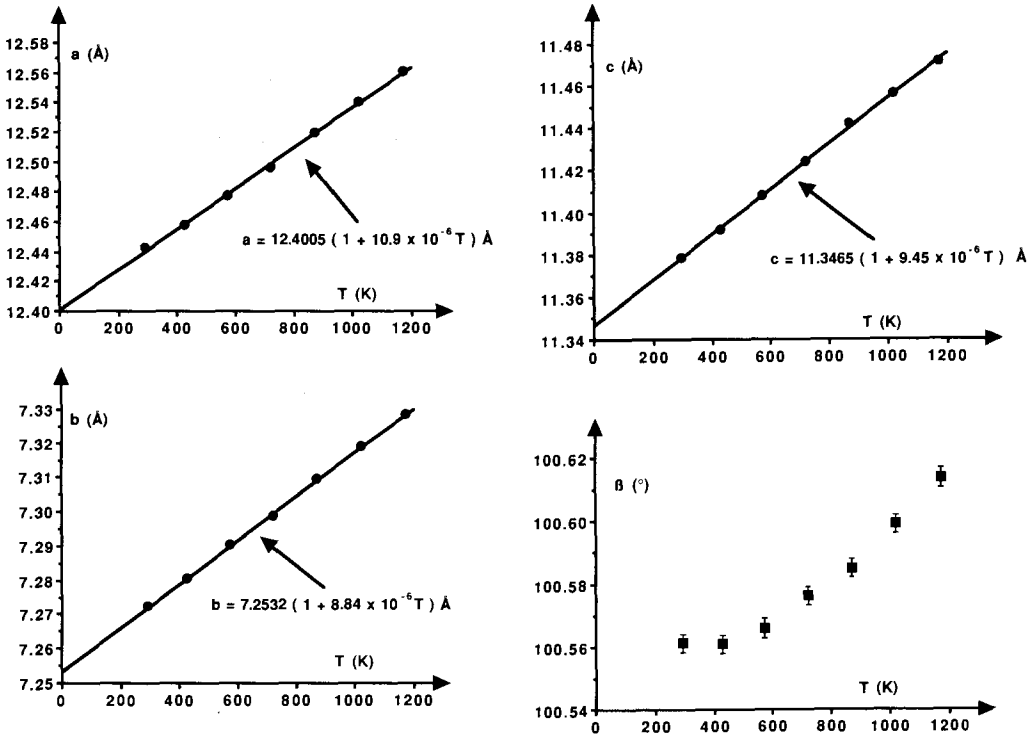

FIG. 2. Monoclinic lattice parameters a, b, c, and β for $CaZr_{0.92}Ti_{2.08}O_7$ plotted against temperature. Except for β, the errors obtained from Rietveld refinement are smaller than the plotting symbols. The plots for a, b, and c were fitted to linear functions of the form $a = a_0(1 + \alpha_a T)$, where a_0 (b_o or c_o) is the lattice parameter at 0 K and α_a (α_b or α_c) is the linear coefficient of expansion (K^{-1}).

the stainless steel canister. All these peaks were excluded from the refinement. The goodness of fit parameter R_{wp} along with its expected value R_{wp}^{exp} and the Bragg R factor R_B are used as the measures of data fit (*12*).

All the patterns were refined according to the space group $C2/c$, as in earlier refinements of zirconolites, and convergence of the refinement was obtained without major problems. Atomic coordinates were assigned according to the scheme of Gatehouse *et al.* (*4*) and independent isotropic temperature factors were used to represent thermal vibrations. All the structural parameters given by refinement are presented in Table I. The composition quoted in this table was obtained by refinement of the occupancies in the data collected at 294 K using the occupancies in (*4*) for $CaZr_{0.85}Ti_{2.15}O_7$ as the starting values. Change balance was incorporated into the refinement and the total occupancy on each site was constrained to ≤ 1. In accordance with the earlier refinement, negligible Zr was observed on the Ti(2) and Ti(3) sites, but in contrast no Zr was observed on the Ca sites. The composition obtained by this method, namely $CaZr_{0.92}Ti_{2.08}O_7$, is consistent with the composition indicated by the lattice parameters and the fact that small amounts of ZrO_2 and $CaTiO_3$ were recorded in the X-ray data. The site occupancies assumed during the refinement of the high temperature data

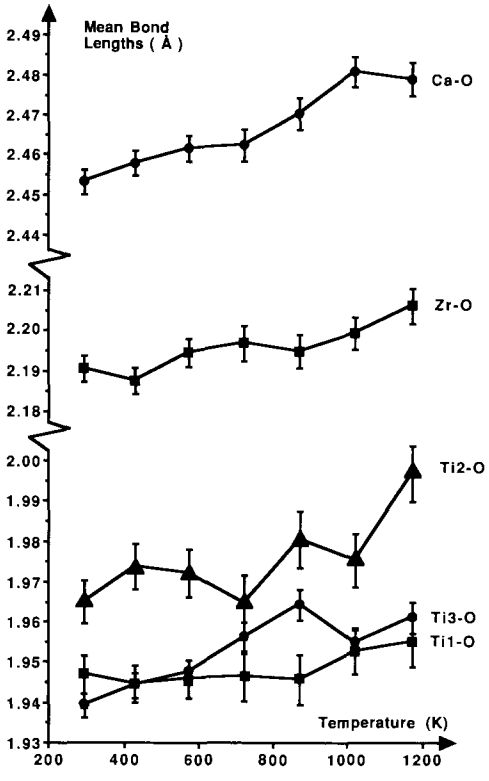

FIG. 3. Variation of the mean bond lengths with temperature in each of the oxygen polyhedra; CaO_8, ZrO_7, $Ti(1)O_6$, $Ti(2)O_5$, and $Ti(3)O_6$.

were

Ca Site	1.00 Ca
Zr Site	0.90 Zr + 0.10 Ti
Ti(1) Site	0.98 Ti + 0.02 Zr
Ti(2) Site	0.50 Ti
Ti(3) Site	0.50 Ti.

Excellent fits were obtained for all the diffraction patterns with R_{wp} in the vicinity of 5% in the high-temperature patterns given expected values $R_{wp}^{exp} \sim 3\%$ and Bragg R factors $R_B \sim 2\%$.

3. Results

There are no large-scale changes in the structural parameters with increasing temperature, and the crystal structure is substantially the same at all temperatures as that described by Gatehouse *et al.* (*4*). The only significant changes arise from normal thermal expansion effects. The lattice parameters a, b, and c increase linearly with temperature, and the similarity of the linear expansion coefficients in each axial direction α_a, α_b, and α_c, indicates that the expansion is essentially isotropic (see Fig. 2). The cell angle β, however, displays some unexplained nonlinearity near room temperature.

The large errors in the fractional coordinates obtained in the present results compared with the X-ray single crystal studies of Gatehouse *et al.* (*4*) preclude a detailed analysis of individual metal–oxygen bond lengths. In this paper only the average bond lengths in the various oxygen polyhedra are discussed (viz. CaO_8, ZrO_7, $Ti(1)O_6$, $Ti(2)O_5$, and $Ti(3)O_6$). The average bond lengths obtained for these polyhedra at 294 K agree well with the room-temperature values of the Ti-rich zirconolite of Gatehouse *et al.* All the present results are incorporated in Fig. 3, where the error bars in each mean bond length $\langle L \rangle$ were obtained using the general error equation,

$$\sigma^2(\langle L \rangle) = \sum_{i=1}^{N} \left(\frac{\partial \langle L \rangle}{\partial u_i} \right)^2 \sigma^2(u_i),$$

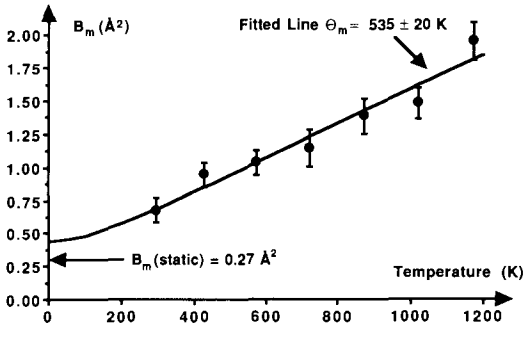

FIG. 4. Mass-weighted temperature factor B_m plotted against temperature and fitted by superimposing a Debye function with $\theta_m = 535 \pm 20$ K on to a temperature-independent static disorder contribution of 0.27 Å^2.

where u_i are the independent structural parameters defining the positions of the ions in the polyhedron. All the polyhedra expand uniformly with temperature with the possible exception of the $Ti(1)O_6$ octahedron, which remains more or less constant in size over the temperature range. The irregularities in the $Ti(2)O_5$ polyhedron growth are not considered to be significant.

No detailed analysis of the individual temperature factors was undertaken except to note that the values at room temperature are substantially the same as Gatehouse *et al.* and that the Ti(2) value is unusually large probably because the site is significantly larger than the Ti ion. It should be noted that neither the Zr nor the Ca site ions have large temperature factors. In the context of radwaste disposal this demonstrates that these ions do not have large amplitudes of vibration and are unlikely to escape from within their respective polyhedra. This is supported by the fact the largest O–O separation in a CaO_8 box does not exceed 4.3 Å even at 1173 K and is considerably less than the 2 × Ca–O bond length at that temperature (i.e. 2 × 2.48 Å). In other words, the "holes" between the oxygens in the surface of the ZrO_7 and CaO_8 polyhedra are smaller than the cations, thereby making the activation energy for a jump by a Zr or Ca ion large.

To minimize the effects of large errors in individual B values and to calculate the X-ray Debye temperature θ_m, the mass weighted mean temperature parameter B_m was analyzed. When extrapolated to $T = 0$ K, B_m is larger than would be expected for thermal effects alone. It was therefore assumed that static disorder contributes to B_m. The Debye temperature θ_m of the present zirconolite and the degree of static disorder were estimated using the method described in (*14*). Figure 4 shows the observed variation of B_m and the optimum Debye function fitted to these observations. This analysis gives $\theta_m = 535 \pm 20$ K and a static disorder contribution to B_m of 0.27 Å^2 which probably arises from mixing different sized ions in the O polyhedra.

4. Conclusions

No significant structural changes occur in zirconolite up to 1200 K other than thermal expansion. The CaO_8 polyhedron is stable at all temperatures and the Ca–O bond (2.45 Å at 294 K) is similar to the bond lengths of rare earth radwaste ions (Nd^{3+}–O = 2.48 Å, Yb^{3+}–O = 2.37 Å). These ions should therefore be incorporated into the zirconolite structure with minimal deformation to the CaO_8 polyhedron. The tight fitting box of oxygens around each Ca site will provide a barrier with a high activation energy.

Acknowledgments

The author acknowledges the financial support of the Advanced Materials Program at the Australian Nuclear Science and Technology Organisation under Research Contract 82/X/1, and the provision of neutron diffraction facilities through the Australian Institute of Nuclear Science and Engineering.

References

1. P. Fielding and T. J. White, *J. Mater. Res.* **2,** 387 (1987).
2. V. M. Oversby and A. E. Ringwood, *Radioact. Waste Manage.* **1,** 289 (1981).
3. W. Sinclair and R. A. Eggleton. *Am. Mineral.* **67,** 615 (1982).
4. B. M. Gatehouse, I. E. Gray, R. J. Hill, and H. J. Rossell, *Acta Crystallogr.* **B37,** 306 (1981).
5. Y. A. Pyatenko and Z. V. Pudovkina, *Sov. Phys. Crystallogr. (Engl. Transl.)* **9,** 76 (1964).
6. H. J. Rossell, *Nature (London)* **283,** 282 (1980).
7. T. J. White, *Am. Mineral.* **69,** 1156 (1984).
8. R. D. Shannon, *Acta Crystallogr.* **A32,** 751 (1976).
9. P. Bayliss, F. Mazzi, R. Munro, and T. J. White, *Mineral. Mag.* **53,** 565 (1989).
10. C. J. Howard, C. J. Ball, Davis, L. D. and M. M. Elcombe, *Aust. J. Phys.* **35,** 507 (1983).
11. D. B. Wiles and R. A. Young, *J. Appl. Crystallogr.* **14,** 149 (1981).
12. C. J. Howard and R. J. Hill, Australian Atomic Energy Commission Report, Lucas Heights Research Laboratories, AAEC/M112 (1986).
13. C. J. Howard, *J. Appl. Crystallogr.* **15,** 615 (1982).
14. R. W. Cheary, *Acta Crystallogr.* **B47,** 312 (1991).